DOI: 10.1002/ejic.200900382

Spontaneous Reduction of High-Spin Fe^{III} Complexes Supported by Benzoic Hydrazide Derivative Ligands

Nouri Bouslimani,[a] Nicolas Clément,[a] Clément Toussaint,[a] Sophie Hameury,[a] Philippe Turek,[b] Sylvie Choua,[b] Samuel Dagorne,[a] David Martel,[c] and Richard Welter*[a]

Keywords: Iron / Reduction / Structure elucidation / Hydrogen bonds / N,O ligands

We report herein experimental evidence for the spontaneous reduction of new high-spin iron(III) $Fe^{III}(L^{(n)})_2Cl$, L complexes to new high-spin iron(II) $Fe^{II}(HL^{(n)})_2Cl_2$ mononuclear complexes. These processes were checked by EPR, cyclovoltammetric, and pseudo-steady voltammetric studies. Crystal structures of three new complexes (one Fe^{III} and two Fe^{II}) were obtained from RX single-crystal diffraction.

Introduction

The coordination chemistry of iron has been studied over many facets over the last 50 years.[1,2] For example, the paramagnetic character of high-spin iron +III and high-spin iron +II has been largely explored in the field of molecular magnetism[3] or mixed-valence system.[4] The spin state as well as the oxidation state of iron strongly depends on the ligand.[5] Ligands with carboxamide or carboxylate groups exhibit preference towards the Fe^{III} ion. Ligands with pyridine and imidazole nitrogen atoms afford stable Fe^{II} complexes.[5] Therefore, specific design of the ligands surrounding the iron center could allow a tuning of the redox and magnetic properties of the designed complexes.

We recently pointed out an unusual spontaneous reduction from Fe^{III} to Fe^{II} of mononuclear complexes supported by a salicyloylhydrazono dithiolane ligand.[6] This unexpected reduction was fully investigated by electrochemistry, EPR studies, magnetic measurements and solid-state molecular structure determination. Considering that closely related dinuclear compounds[7] can exhibit strong ferromagnetic coupling, such a spontaneous reduction phenomenon opens up new research opportunities, as recently pointed out by Wernsdorfer et al.[8] Thus, provided this reduction process is understood and well controlled, such molecular complexes may offer the possibility to tune the magnetic coupling exchange by changing the spin state, especially if this can be induced by external stimuli.[9]

In an effort to gain more insight into the structural factors controlling and influencing the spontaneous reduction of Fe^{III} to Fe^{II} observed for Fe mononuclear species, the original ligand was modified at specific positions. In the present article, we report on the synthesis and structural characterization of three novel iron compounds supported by benzoic hydrazide ligand derivatives (Scheme 1). The new cases of spontaneous reduction $Fe^{III} \rightarrow Fe^{II}$ were checked by electrochemistry and EPR spectroscopy.

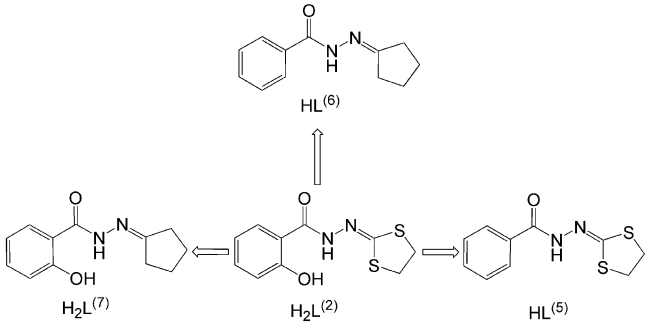

Scheme 1. Structural modifications of the original ligand $H_2L^{(2)}$.

Results and Discussion

Synthesis and Structural Characterization

The initial task of the present work dealt with the synthesis of the benzoic hydrazide ligand derivatives that are related to the original ligand we used (2-salicyloylhydrazono-

[a] Laboratoire DECOMET, Institut de Chimie, UMR 7177 CNRS, Université de Strasbourg,
4, rue Blaise Pascal, 67070 Strasbourg cedex, France
Fax: +33-90-24-12-29
E-mail: welter@chimie.u-strasbg.fr
[b] Laboratoire POMAM, UMR 7177 CNRS, Université de Strasbourg,
1, rue Blaise Pascal, 67008 Strasbourg cedex, France
[c] Laboratoire d'Electrochimie et de Chimie Physique du Corps Solide, UMR 7177 CNRS, Université de Strasbourg,
67070 Strasbourg cedex, France

Supporting information for this article is available on the WWW under http://dx.doi.org/10.1002/ejic.200900382.

1,3-dithiolane), yet being slightly modified. The ligands $HL^{(5)}$, $HL^{(6)}$, and $H_2L^{(7)}$ were prepared according to literature procedures.[10,11]

Iron Complexes Supported by the $L^{(5)-}$ Bidentate Ligand

$FeCl_3$ was used in the present studies as our primary Fe^{III} source. The reaction of the ligand $HL^{(5)}$ with $FeCl_3$ in DMF yields a dark-blue solution of the complex $Fe(L^{(5)})_2DMF$ (**1a**, Scheme 2). Complex **1a** was isolated in the solid state as dark-blue crystals after diffusion of diethyl ether into a DMF solution in air in a reasonable yield. When the diffusion of diethyl ether into the DMF solution of **1a** is carried out very slowly in a sealed glass tube under an inert N_2 atmosphere, a color change is observed. In fact, within a few days, the solution color gradually changes from dark blue to light yellow. Upon air exposure, the latter solution turns back to its original dark-blue color within a few seconds. Despite numerous attempts, single crystals suitable for X-ray analysis could not be obtained from this yellow solution. Nevertheless, a closely related phenomenon has recently been described by us, and this color change corresponds to a spontaneous reduction of Fe^{III} to Fe^{II}, as was unambiguously confirmed by electrochemical measurements as well as EPR studies (see below).[6] On this basis, it is very likely that the present color change arises from the conversion of complex **1a** (Fe^{III}, dark blue) to **1b**, a Fe^{II} light-yellow compound in DMF solution. Interestingly, this reduction appears to be reversible, as **1b** may be rapidly converted back **1a** by exposure to air. Scheme 2 summarizes the different transformations observed and analyzed for iron complexes supported by $HL^{(5)}$.

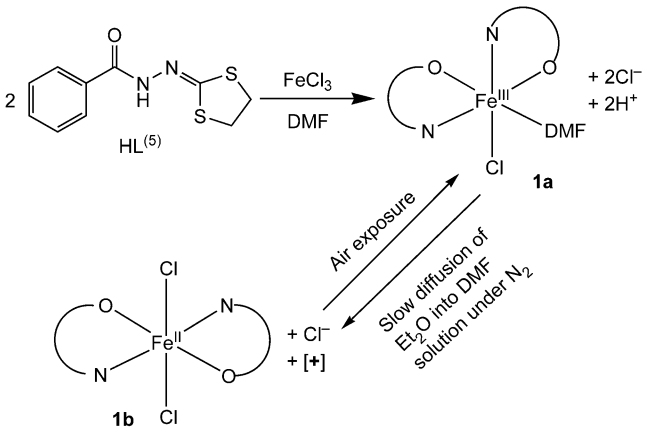

Scheme 2. Main transformations observed for the complexes obtained with the ligand $HL^{(5)}$. [+] represent the oxidant formed during the spontaneous reduction of complex **1a**.

Complex **1a**, isolated as suitable single crystals for X-ray analysis, crystallizes in the centrosymmetric space group $P2_1/n$ as a mononuclear Fe^{III} species, in which the central Fe atom adopts an octahedral geometry (Figure 1). Both $L^{(5)}$ ligands (the absence of hydrogen atom on N1 and N3 is unambiguously observed by X-ray diffraction) are in a *cis* configuration and the deformed octahedral environment is completed by one chloride atom and one DMF solvent molecule. No classical hydrogen bond appears to be present in this crystal structure; the presence of a non-negligible CH–π interaction involving C19 and the C12–C17 phenyl ring centroid of the adjacent molecule (with the following symmetry operator: x, $-1/2 - y$, $1/2 + z$), should, however, be noted.

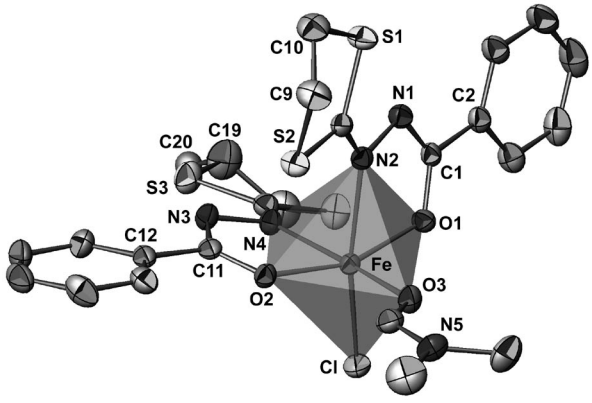

Figure 1. ORTEP view of complex **1a** with partial labeling scheme. The ellipsoids enclose 50% of the electronic density. Selected bond lengths [Å] and angles [°]: Fe–O1 1.968(2), Fe–O2 1.982(2), Fe–O3 2.057(2), Fe–N4 2.135(2), Fe–N2 2.217(2), Fe–Cl 2.270(1), O2–Fe–O1 161.2(1), N2–Fe–Cl 167.5(1).

Iron Complexes Supported by the $L^{(6)-}$ Bidentate Ligand

Complex **2a** was prepared by direct reaction of $HL^{(6)}$ and $FeCl_3$ in DMF. Unfortunately, no suitable single crystals of **2a** could be grown thus far despite numerous attempts; nevertheless, electrochemical measurements as well as EPR studies are strongly consistent with **2a** consisting of a mononuclear Fe^{III} complex with chelating $L^{(6)-}$ ligands, DMF and/or Cl in the direct coordination sphere of iron ion (vide infra and Experimental Section).

Similar to previous observations for the $(L^{(5)})_2Fe^{III}$-type complexes **1a** and **1b** (vide supra), slow diffusion of diethyl ether into a DMF solution of complex **2a** (sealed glass tube, N_2 atmosphere) induced a gradual color change (from blue–purple to yellow) over the course of a few days. A fair amount of yellow single crystals of **2b** (suitable for X-ray studies) were found to have formed at the bottom of tube when the diffusion process is over. The solid-state molecular structure of compound **2b** (Figure 2) was thus established by X-ray crystallographic studies, identifying **2b** as a Fe^{II} mononuclear species. In the latter complex, the metal center (Fe^{II} located on the crystallographic inversion center) is surrounded by two neutral $HL^{(6)}$ ligands and two chloride atoms in a *trans* position to one another (Figure 2). The overall structure of **2b** appears to be very similar to that recently published by our group.[6] Importantly, complex **2b** constitutes so far the second example of a high-spin Fe^{II} species derived from spontaneous reduction of a high-spin Fe^{III} species, the former complex being stable and charac-

terized both in solution and crystalline solid states (see also EPR and Electrochemical Measurements section). It is noteworthy that single crystals of complex **2b** are air stable for weeks. This can probably be related to the numerous hydrogen bonds [N1–H1N···Cl′ 2.46(3) Å, 178(3)°; C7–H7···Cl′, 2.75(3) Å, 137(3)°; C12–H12A···Cl′, 2.78(3) Å, 124(3)°, where ′ = 1 –*x*, –*y*, 1 – *z*] as well as CH–π interactions [C9–H9B···phenyl-centroid′: 3.01(3) Å, 142(3)°] found in this crystal structure; these interactions undoubtedly account for the good stability of complex **2b** in the crystalline state.

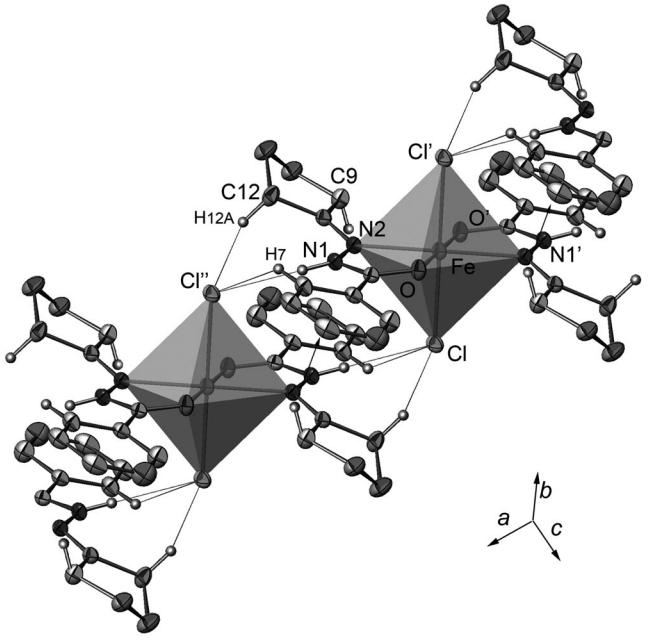

Figure 2. Expanded ORTEP view of complex **2b** with partial labeling scheme. Ellipsoids enclose 50% of the electronic density. The thin lines indicate principal hydrogen bonds. Arrows indicate CH–π interactions. Selected bond lengths [Å] and angles [°]: Fe–O 2.152(2), Fe–Cl 2.435(1), Fe–N2 2.200(2), N1–N2 1.405(2), O–Fe–Cl 87.41(7), N2–Fe–Cl 91.64(6). Symmetry operator for equivalent positions: ′ = –*x*, –*y*, –*z* + 1; ′′ = 1 – *x*, –*y*, 1 – *z*.

Iron Complexes Supported by the HL$^{(7)-}$ Bidentate Ligand

Complex **3a** (light brown) was prepared by reaction of the neutral proligand $H_2L^{(7)}$ with $FeCl_3$ following the same procedure described in Scheme 2 for complex **1a**. Here again, no suitable single crystals of **3a** could be grown: nevertheless, electrochemical measurements as well as EPR studies strongly suggest that **3a** is a mononuclear Fe^{III} bearing two $HL^{(7)-}$ bidentate ligands (vide infra). Akin to the case of the two similar mononuclear Fe^{III} complexes **1a** and **2a**, slow and anaerobic crystallization of complex **3a** afforded single crystals of the mononuclear Fe^{II} species **3b** (deep yellow, in a reasonable yield), whose solid-state molecular structure was determined by X-ray crystallographic studies. Thus, the preparation of complex **3b** from **3a** constitutes another example of a readily formed high-spin Fe^{II} species from spontaneous reduction of high-spin Fe^{III} species.

As illustrated in Figure 3, the molecular structure of **3b** is very similar to that of **2b** and numerous hydrogen bonds as well as CH–π interactions have been detected. The redox properties of this complex were investigated by voltammetric techniques and unambiguously confirmed the oxidation state of the metal center. EPR studies carried out on these crystals are also consistent with a high-spin Fe^{II} species (vide infra). Complex **3b** is moderately air stable in the crystalline state and presumably oxidizes upon air exposure; it is also quite unstable in solution under aerobic conditions and undergoes rapid oxidation. Thus, solutions of **3b** had to be handled under strictly anaerobic conditions.

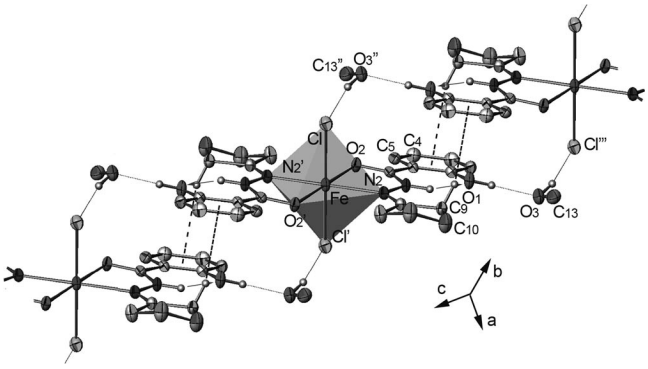

Figure 3. Expanded ORTEP view of complex **2b** with partial labeling scheme. Ellipsoids enclose 50% of the electronic density. The thin lines indicate principal hydrogen bonds. Arrows indicate CH–π interactions. Selected bond lengths [Å] and angles [°]: Fe–O 2.152(2), Fe–Cl 2.435(1), Fe–N2 2.200(2), N1–N2 1.405(2), O–Fe–Cl 87.41(7); N2–Fe–Cl 91.64(6). Symmetry operator for equivalent positions: ′ = –*x*, –*y*, –*z* + 1; ′′ = 1 – *x*, –*y*, 1 – *z*. Expanded ORTEP view of complex **3b** with partial labeling scheme. Ellipsoids enclose 50% of the electronic density. Dashed lines and arrows indicate both hydrogen bonds and CH–π interactions. Selected bond lengths [Å] and angles [°]: Fe–O2 2.169(2), Fe–Cl 2.449(1), Fe–N2 2.191(2), O2–Fe–Cl 92.93(4); N2–Fe–Cl 89.05(5). Symmetry operator for equivalent positions: ′ = –*x* + 1, –*y*, –*z*; ′′ = 2 – *x*, 1 – *y*, –*z*; ′′′ = *x*, –1 + *y*, *z*.

Evidence from Electrochemical Studies for the Spontaneous Reduction Process $Fe^{III} \rightarrow Fe^{II}$

All six complexes, **1a/1b**, **2a/2b**, and **3a/3b**, were investigated by cyclic voltammetry and quasi-steady state. Figure 4 highlights the obtained results showing the pseudo-steady-state curves in the inset.

In cyclic voltammetry, the reduction of the Fe^{III} complexes (full line) presents very similar behavior; that is, the influence of ligands on the reduction properties of these complexes seems to be marginal. In contrast, the reoxidation of the electrogenerated Fe^{II} complexes shows differences depending on the ligands: whereas only one peak is observed with the **2a/2b** system, two peaks are observed for both systems **1a/1b** and **3a/3b**. This behavior is confirmed when the Fe^{II} complexes are studied (dotted line): the oxidation part of the cyclic voltammograms features very similar signals to that of the reoxidation of the electrogenerated Fe^{II} complexes from Fe^{III}. However, in the case of complex

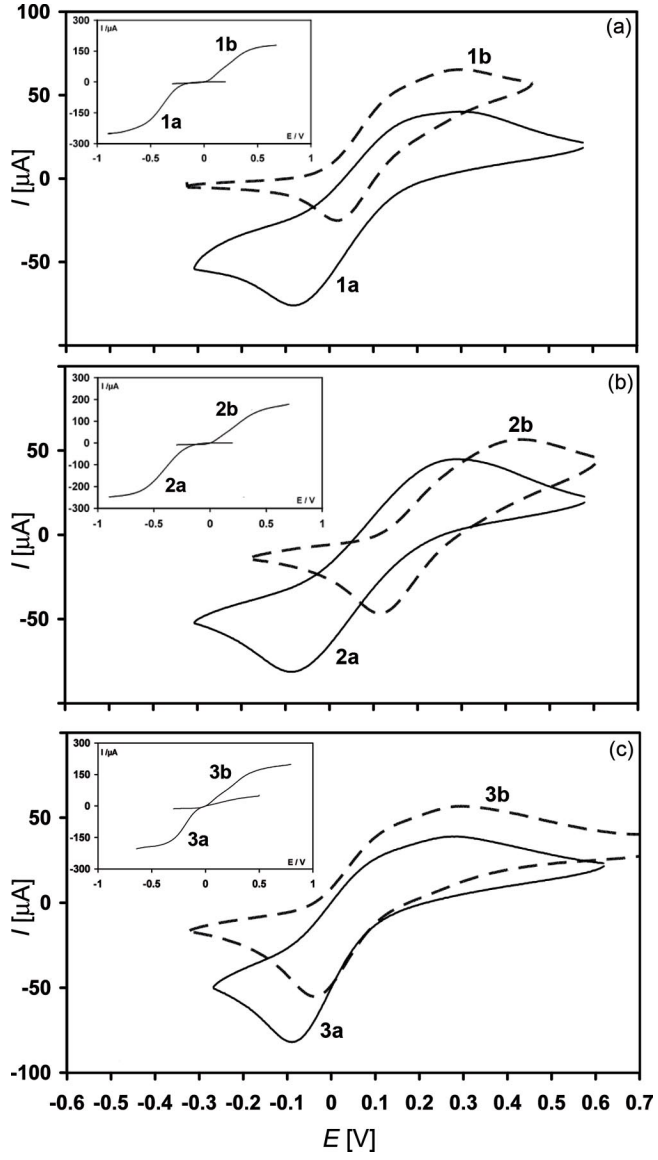

Figure 4. Cyclic voltammograms of complexes supported by $HL^{(5)}$ (a), $HL^{(6)}$ (b), and $H_2L^{(7)}$ (c) (10 mM) in DMF with supporting electrolyte nBu$_4$PF$_6$ 0.15 M, scan rate 0.1 V s^{-1}. Dashed curves were obtained starting from Fe^{II} complexes and solid line curves from Fe^{III} complexes. Insert: quasi-steady state current potential curves for each complex in DMF with supporting electrolyte nBu$_4$PF$_6$ 0.15 M, scan rate: 2 mV s^{-1}, rotation rate: 1000 rpm.

2b and unlike what is observed for complexes **1b** or **3b**, one peak is observed but shifted in potential toward more positive values. These data indicate that it is more difficult to oxidize complex **2b** than the two others.

The rereduction of the electrogenerated Fe^{III} complexes also presents some variation, dependent upon the considered complex, and the data are comparable to those for the reduction of the Fe^{III} complexes (initially present in solution). In the case of complexes supported by $H_2L^{(7)}$ ligand, the Fe^{III} difference in peak reduction potentials is 42 mV. In the case of complexes supported by the $HL^{(5)}$ ligand, this difference is 100 mV, and with $HL^{(6)}$ ligand, it is 200 mV. This indicates that it is easier to reduce the electrogenerated complexes in the following order: **2a**, **1a**, and **3a**. All these data are consistent with an important influence of the ligands on the electrochemical behavior of the presently studied Fe^{III}/Fe^{II} systems.

Two parameters could be pointed out in order to rationalize the observed results. First, an equilibrium may exist between FeL_2 and FeL in solution, which is related to the redox state of the metal and the nature of the ligand. Second, the change in conformation of the iron complexes may influence the electronic level and modified the electrochemical behavior. These two parameters might influence the electrochemical signal.

Finally, using quasi-steady-state voltammetry, the redox state of the Fe metal centers was unambiguously confirmed. In all cases, when a Fe^{III} complex was present in bulk solution, a reduction signal was obtained (without an oxidation signal), whereas no reduction signal was observed for the Fe^{II} complexes (only an oxidation signal was detected).

Evidence from EPR Studies for the Spontaneous Reduction Process $Fe^{III} \rightarrow Fe^{II}$

The reversible and spontaneous reduction/oxidation processes ($Fe^{III} \rightarrow Fe^{II}$ and $Fe^{II} \rightarrow Fe^{III}$) for the synthesized iron complexes were also evidenced by EPR measurements.

In the case of the **1a/1b** system, the solid-state structure of mononuclear Fe^{III} complex **1a** clearly indicates a +III oxidation state for the iron metal center, which is further confirmed by EPR measurements. The low-temperature (4 K) EPR spectrum of **1a** (Figure 5c) is characterized by a typical signal of a high-spin state (S = 5/2). The hypothetical mononuclear Fe^{II} species **1b** is obtained after slow diffusion of diethyl ether into the dark-blue DMF solution of complex **1a** under strictly anaerobic conditions to yield a light-yellow solution. As discussed above, the same color change was reported for the original system $Fe^{III}(HL^{(2)})_2$/$Fe^{II}(H_2L^{(2)})_2$; however, in this case, the solid-state molecular structure of $Fe^{II}(H_2L^{(2)})_2$ could be determined.[6] Unfortunately, in the **1a/1b** system, no single crystals of the reduced species (i.e., **1b**) could be grown: the +II oxidation state of this hypothetical mononuclear species (corresponding to the yellow solution) can nevertheless clearly be deduced from electrochemical data (vide supra).

EPR measurements confirmed the putative structure of **1b**. Thus, the low-temperature (4 K) EPR spectrum of the aforementioned yellow solution (Figure 5a) shows a hump at low field ($g_{eff} \approx 31$) and a set of signals peculiar for a high-spin Fe^{III} (S = 5/2) species originating from a trifling oxidation of the solution, as the yellow solution is very sensitive to oxidation; that is, the mononuclear complex is more stable in the (+III) oxidation state than (+II). The signal at $g_{eff} \approx 31$ most likely originates from a Fe^{II} species. The recovery of the dark-blue color of the initial solution is readily achieved upon air exposure of the yellow solution, indicating the oxidation of the mononuclear Fe^{II} species into Fe^{III}. The EPR spectrum of this resulting dark-blue solution (recorded a few minutes after air exposure of the

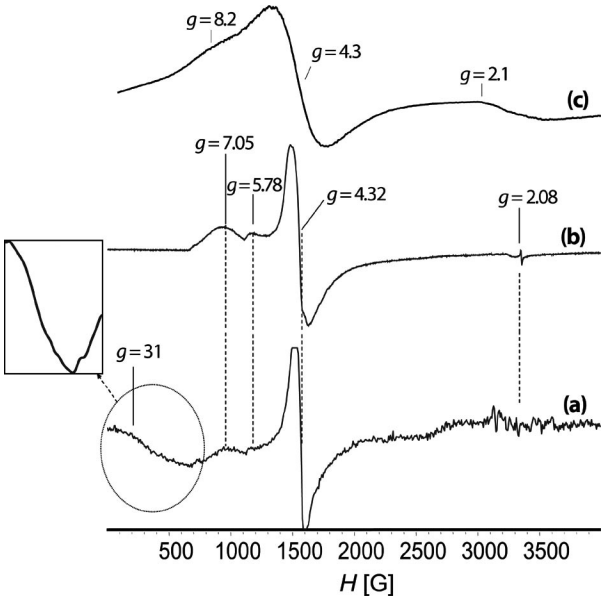

Figure 5. (a) 4 K EPR spectrum of the DMF yellow solution (≈10^{-3} M) of **1b** (slightly oxidized); (b) 4 K EPR spectrum of the DMF blue solution (≈10^{-3} M) of **1b** after air exposure; (c) 4 K EPR spectrum of **1a** (polycrystalline).

yellow solution) clearly shows a rhombic signal typical of a high-spin Fe^{III} species with a g tensor (g_1, g'_1 = 7.05, 5.78, g_2 = 4.32, and g_3 = 2.08), (this second component g'_1 of the rhombic g tensor is probably due to the existence of more than one mononuclear Fe^{III} species in the solution, in accordance with electrochemistry investigations.) (Figure 5b).

The mononuclear Fe^{II} complex in the solid crystalline state is readily obtained with ligands $H_2L^{(7)}$ (**3b**) and $HL^{(6)}$ (**2b**), as discussed previously (evidenced by both crystal structure and voltammetric studies). This is further supported by EPR studies indicating a high spin (S = 2) Fe^{II} center for both complexes **2b** and **3b**, and this was previously supported by magnetometric measurements.[6] Such integer spin systems (namely non-Kramers system) are expected to be EPR silent at conventional fields and frequencies (X-band, 9.4 GHz and Q-band, 35 GHz).[12–14] However, in some cases of low symmetry (from axial to rhombic), transitions involving $|\Delta Ms| > 1$ (formally EPR forbidden) may become partially "EPR allowed" and are EPR visible particularly when parallel mode detection is used.[14] Such an opportunity is attributed to a spread in zero-field-splitting (ZFS) values due to, for example, disorder, which makes it possible to observe transitions arising from a fraction of molecules.

In the present investigation, the default perpendicular mode is used. The low-temperature (4 K) EPR spectrum performed on a polycrystalline powder of complex **3b** (Figure 6a) exhibits a prominent signal at g_{eff} = 9.4 with a tiny signal at g = 4.3 and a very broad feature around g = 2. No other features are observed up to 1 T. We can safely attribute the g = 4.3 and g = 2 signals to a minority high-spin Fe^{III} species resulting from a trifling oxidation of the surfaces of the crystals, as it represents a small fraction of the total intensity. According to the frame presented above,[13] the position and the lineshape of the g = 9.4 line are indicative of a high-spin (S = 2) Fe^{II} state, thus evidencing the $Fe^{III} \leftrightarrow Fe^{II}$ interconversion. According to previous theoretical work,[13,14] the observed spectrum should be attributed to a ground doublet, presumably $|2,2^{\pm}\rangle$, with a rhombic dipolar tensor (E/D ≠ 0), to allow for a splitting of this ground doublet. No striking features were observed at increasing temperatures (25 to 150 K) except for signals presumably originating from other Ms values within the S = 2 manifold (see Supporting Information). These are not discussed here, as the 4 K spectrum is convincing enough to show the interconversion between Fe^{III} and Fe^{II}.

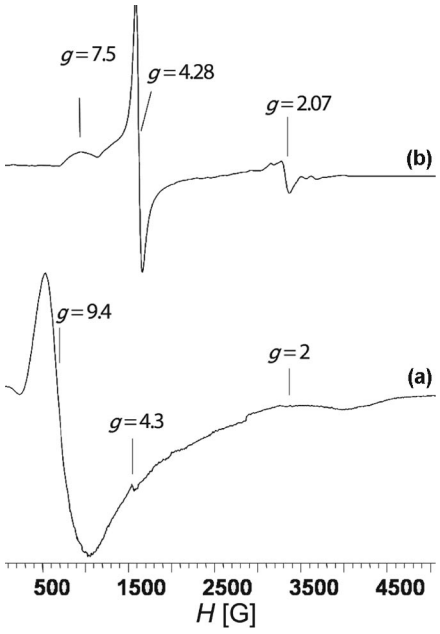

Figure 6. (a) 4 K EPR spectrum of complex **3b** (powder); (b) 4 K EPR spectrum of a DMF solution of **3b** (≈10^{-3} M), a few minutes after air exposure.

When the polycrystalline powder of **3b** is dissolved in DMF for instance, without special care with regards to anaerobic conditions, the solution changes color (from deep yellow to dark brown) within few seconds, indicating the conversion from Fe^{II} (**3b**) to Fe^{III} species (**3a**) (Figure 6b).

The behavior of the complex $Fe^{II}(L^{(6)})_2Cl_2$ (**2b**) in the polycrystalline state is quite similar to that of $Fe^{II}(HL^{(7)})_2Cl_2$ (**3b**) discussed above. The EPR spectrum of the polycrystalline powder of complex **2b** recorded at low temperature (4 K; Figure 7a) exhibits a single broad line in the low-field region (g_{eff} = 21). No other features were observed up to 1 T. According to the frame of discussion for compound **3b**, the peculiarities of this signal agrees with a high-spin Fe^{II} (S = 2) complex. The larger g value for the spectrum of complex **2b** may indicate a larger rhombicity (E/D ratio) of the ZFS tensor, and hence a lower symmetry around the iron center.[14]

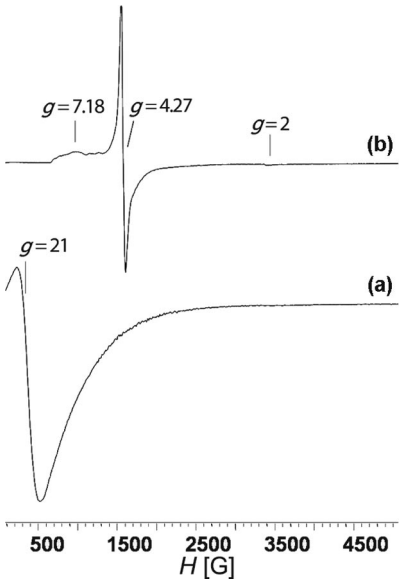

Figure 7. (a) 4 K EPR spectrum of complex **2b** (powder); (b) 4 K EPR spectrum of a DMF solution of **2b** (≈10^{-3} M), a few minutes after air exposure.

The low-temperature (4 K) EPR spectrum of the solution obtained after dissolving the polycrystalline powder of complex **2b** in DMF and exposed to air is depicted in Figure 7b. The spectrum shows a typical signal of a high-spin Fe^{III} species with a rhombic g tensor (g_1 = 7.18, g_2 = 4.27, g_3 = 2). No other signals were observed up to 1 T. The Fe^{III} species were generated in situ upon air exposure of the solution. Except for the intensity decrease of the main line (g = 4.27), no other features are observed at higher temperature until the whole signal disappears above 100 K.

Concluding Remarks

The main result of this work concerns the spontaneous reduction of three novel high-spin Fe^{III} complexes $Fe^{II-I}(L^{(n)})_2Cl$, L (**1a**, **2a**, and **3a**, L = solvent) to the corresponding high-spin Fe^{II} mononuclear complexes $Fe^{II}(HL^{(n)})_2Cl_2$ (**1b**, **2b**, and **3b**). These amazing processes were evidenced by EPR studies, cyclovoltammetry, and pseudo-steady voltammetry. Yet, to date, the reduction process remains unclear to us, but considering that all these complexes are supporting closely related ligands, the origin of this phenomenon may be related to the ligand backbone structure. The stability of the reduction products, that is, the high-spin Fe^{II} complexes $Fe^{II}(HL^{(n)})_2Cl_2$, is likely to be one of the driving forces in these spontaneous reductions processes. One should also point out that a few related Fe^{III}–Fe^{II} reductions have been reported in the literature,[15–17] including the spontaneous reduction of salicylido-type iron(III) complexes to iron(II) analogs,[18] which was proposed to proceed via radical pathways.[19–22] Accordingly, the present spontaneous reductions may also involve radical processes. Further studies in this area will be aimed at gaining insight into the mechanism of the above reductions through in situ EPR measurements. Overall, the *reversible and spontaneous* reduction processes described in this present work open up a very broad scope of new opportunities for further investigations, especially concerning magnetic systems in which one could tune the magnetic interactions as a function of the redox state of the metal center.

Experimental Section

General: All manipulations were performed under aerobic conditions by using reagents and solvents as received, unless specified otherwise. Synthetic details are presented only for the complexes obtained in single-crystal form.

$Fe(L^{(5)})_2DMF{\cdot}Cl$ (1a): To a well-stirred solution of $HL^{(5)}$ (71.5 mg, 0.3 mmol) in DMF (2 mL) was added $FeCl_3$ (16.2 mg, 0.1 mmol). After 5 h of stirring at room temperature, diethyl ether (8 mL) was layered carefully onto the surface of the dark-blue solution and then left undisturbed for slow precipitation (2–3 d). The resulting dark crystalline powder of the title complex was collected by filtration and washed with diethyl ether. Yield: 35 mg, 55%. $C_{23}H_{25}ClFeN_5O_3S_4{\cdot}1/2Et_2O$: calcd. C 40.85, H 3.70, N 10.36; found C 40.71, H 3.68, N 10.15.

$Fe(HL^{(6)})_2(Cl)_2$ (2b): To a well-stirred solution of $HL^{(6)}$ (60 mg, 0.3 mmol) in DMF (2 mL) was added $FeCl_3$ (16.2 mg, 0.1 mmol), and the mixture was then stirred for 6 h at room temperature. The resulting crude blue–purple solution was then layered carefully with diethyl ether (10 mL) in a sealed glass tube to afford the title complex as deep-yellow crystals after a slow diffusion within 2–4 d. Yield: 22 mg, 42%. $C_{24}H_{26}Cl_2FeN_4O_2$ (529.25): calcd. C 54.47, H 4.95, N 10.60; found C 54.25, H 5.23, N 11.0.

$Fe(H_2L^{(7)})_2(Cl)_2$ (3b): To a well-stirred solution of $H_2L^{(7)}$ (65.5 mg, 0.3 mmol) in MeOH (5 mL) was added a solution of $FeCl_3$ (16.2 mg, 0.1 mmol) in MeOH (2 mL), and the mixture was then stirred for 6 h at room temperature. The complex was obtained as light-brown to deep-yellow crystals after slow diffusion (within 2–4 d) of diethyl ether into the methanolic solution of the crude product in a sealed glass tube. Yield: 15 mg, 30%. $C_{24}H_{26}Cl_2FeN_4O_4{\cdot}MeOH$: calcd. C 50.7, H 5.05, N 9.45; found C 50.8, H 5.04, N 9.40.

EPR Measurements: The EPR spectra were recorded at X-band (ca. 9.8 GHz) with an ESP-300E spectrometer (Bruker) equipped with a rectangular TE 102 cavity and an ESR 900 continuous flow cryostat for liquid He circulation (Oxford). The static field was controlled with a Hall probe, whereas the microwave frequency was simultaneously recorded with a frequency counter (HP-5350 B). Dilute solutions (ca. 10^{-3} mol) were degassed with argon before recording the spectra.

Electrochemistry: Dimethylformamide (DMF) was used as solvent. Before used, DMF was in contact with molecular sieves for 12 h. Tetrabutylammonium hexafluorophosphate; nBu$_4$NPF$_6$ (Fluka, electrochemical grade) was used as supporting electrolyte. All electrochemical measurements were carried out at ambient temperature (20 ± 2 °C) in a classical one-compartment, three-electrode cell. The working electrode was a glassy carbon electrode (3 mm diameter), the counterelectrode was a carbon wire and platinum wire was used as pseudo reference. The potential was calibrated versus the ferrocene system (in our study +0.48 V). The cell was connected to a PGSTAT 20 potentiostat (Eco Chemie, Holland). Argon was bubbled through the solutions prior to measurements.

Table 1. Crystal data and X-ray structure refinement parameters at 173 K for mononuclear complexes **1a**, **2b** and **3b**·2MeOH.

	1a	**2b**	**3b**·2MeOH
Formula	$C_{23}H_{25}ClFeN_5O_3S_4$	$C_{24}H_{27}Cl_2FeN_4O_2$	$C_{26}H_{36}Cl_2FeN_4O_6$
Formula weight [g mol^{-1}]	639.02	530.25	627.34
Crystal system	monoclinic	triclinic	monoclinic
Space group	$P2_1/c$	$P\bar{1}$	$P2_1/c$
a [Å]	19.135(4)	6.981(5)	7.6050(2)
b [Å]	9.549(2)	9.235(5)	10.1380(3)
c [Å]	16.404(6)	10.309(5)	18.7540(5)
α [°]	90	110.71(5)	90
β [°]	99.6280(11)	93.10(5)	99.486(2)
γ [°]	90	99.24(5)	90
V [Å^3]	2955.1(14)	609.2(7)	1426.15(7)
Z	4	1	2
$D_{calcd.}$ [g cm^{-3}]	1.436	1.445	1.461
μ(Mo-K_α) [mm^{-1}]	0.917	0.867	0.763
F(000)	1316	275	656
Crystal size [mm]	0.14 × 0.12 × 0.06	0.20 × 0.10 × 0.05	0.14 × 0.10 × 0.10
θ_{min}–θ_{max}	1.08–30.03	2.13–27.49	2.20–29.11
Data set [h, k, l]	–26/26, –11/13, –16/23	–9/8, –11/10, –13/13	–10/10, –13/12, –25/25
Total, unique data, R_{int}	20813, 8640, 0.0488	5360, 2764, 0.0585	6776, 3826, 0.0431
Observed data [$I > 2\sigma(I)$]	5834	2357	2690
No. reflections, No. parameters	8640, 334	2764, 154	3826, 178
R_2, R_1, wR_2,	0.0893, 0.0529,	0.0467, 0.0371, 0.1109,	0.0850, 0.0498, 0.1067,
wR_1, Goof	0.1531, 0.1416, 1.062	0.1031, 1.077	0.0960, 0.984
Max. and av. shift/error	0.002, 0.000	0.000, 0.000	0.000, 0.000
Min,max. residual density [e Å^{-3}]	–0.617, 0.439	–0.875, 0.387	–0.371, 0.378

Crystal Structure Determinations: Single crystals of complexes **1a**, **2b**, and **3b**·2MeOH were mounted on a Nonius Kappa-CCD area detector diffractometer (Mo-K_α, λ = 0.71073 Å). The complete conditions of data collection (Denzo software[23]) and structure refinements are given in Table 1. The cell parameters were determined from reflections taken from one set of 10 frames (1.0° steps in phi angle), each at 20 s exposure. The structures were solved by direct methods (SHELXS97) and refined against F^2 using the SHELXL97 and CRYSTALBUILDER software.[24,25] The absorption was not corrected. All non-hydrogen atoms were refined anisotropically. Hydrogen atoms were generated according to stereochemistry and refined using a riding model in SHELXL97. In the case of complex **1a** refinement, a squeeze procedure was applied considering a strong disorder on the solvent molecule (diethyl ether). CCDC-719691 (for **1a**), -719693 (for **2b**), and -719696 (for **3b**·2MeOH) contain the supplementary crystallographic data for this paper. These data can be obtained free of charge from The Cambridge Crystallographic Data Centre via www.ccdc.cam.ac.uk/data_request/cif.

Supporting Information (see footnote on the first page of this article): Fully labeled ORTEP views; supplementary EPR spectra; UV spectra for complexes **1a**, **2a**, and **3a**; list of hydrogen bonds and CH–π interactions.

Acknowledgments

We thank the Centre national de la recherche scientifique (CNRS) and the Ministère de la Recherche (Paris) for a PhD grant to N.C. and the Agence Nationale de la Recherche (ANR contract no. ANR-06-JCJC-0008) for funding. We also thank Mohamed Lagzaoui for his help in samples preparation. Mr. Maxime Bernard is gratefully acknowledged for assistance in the EPR experiments and H. N. Cong for his help during electrochemistry measurements.

[1] D. Nicholls in *Comprehensive Inorganic Chemistry* (Eds.: J. C. Emeleus Jr, H. J. Bailar, R. Nyholm, A. F. Trotman-Dickenson), Pergamon, Oxford, **1973**, vol. 3, pp. 979–1051.
[2] a) S. M. Nelson in *Comprehensive Coordination Chemistry* (Ed.: G. Wilkinson), Pergamon, Oxford, **1987**, vol. 4, pp. 217–276; b) P. N. Hawker, M. V. Twigg in *Comprehensive Coordination Chemistry* (Ed.: G. Wilkinson), Pergamon, Oxford, **1987**, vol. 4, pp. 1179–1288.
[3] O. Kahn, *Molecular Magnetism*, Wiley-VCH, New York, **1993**.
[4] Y. Zhao, D. Guo, Y. Liu, C. He, C. Duan, *Chem. Commun.* **2008**, 5725–5727.
[5] A. K. Patra, M. M. Olmstead, P. K. Mascharak, *Inorg. Chem.* **2002**, *41*, 5403–5409 and references cited therein.
[6] N. Bouslimani, N. Clément, G. Rogez, P. Turek, M. Bernard, S. Dagorne, D. Martel, H. N. Cong, R. Welter, *Inorg. Chem.* **2008**, *47*, 7623–7630.
[7] C. Beghidja, G. Rogez, J. Kortus, M. Wesolek, R. Welter, *J. Am. Chem. Soc.* **2006**, *128*, 3140–3141.
[8] L. Bogani, W. Wernsdorfer, *Nat. Mater.* **2008**, *7*, 179–186.
[9] S. Lamansky, P. Djurovitch, D. Murphy, F. Abdel-Razzaq, H. E. Lee, C. Adachi, P. E. Burrows, S. R. Forrest, M. E. Thompson, *J. Am. Chem. Soc.* **2001**, *123*, 4304–4312.
[10] C. Beghidja, M. Wesolek, R. Welter, *Inorg. Chim. Acta* **2005**, *358*, 3881–3888.
[11] M. Okimoto, T. Chiba, *J. Org. Chem.* **1990**, *55*, 1070–1076.
[12] M. P. Hendrich, P. G. Debrunner, *Biophys. J.* **1989**, *56*, 489–506.
[13] F. E. Mabbs, D. Collison, *Electron Paramagnetic Resonance of d Transition Metal Compounds, Studies in Inorganic Chemistry*, Elsevier, Amsterdam, **1992**, vol. 16.
[14] H. Andres, E. L. Bominaar, J. M. Smith, N. A. Eckert, P. L. Holland, E. Münck, *J. Am. Chem. Soc.* **2002**, *124*, 3012–3025.
[15] P. G. David, *J. Chem. Soc., Chem. Commun.* **1972**, 1294.
[16] A. K. Patra, M. M. Olmstead, P. K. Mascharak, *Inorg. Chem.* **2002**, *41*, 5403–5409.
[17] L. A. Eguchi, P. Saltman, *Inorg. Chem.* **1987**, *26*, 3665–3669.

[18] N. Wang, Y. Xu, L. Zhu, X. Shen, H. Tang, *J. Photochem. Photobiol. A: Chem.* **2009**, *201*, 121–127.
[19] J. Sima, L. Horvathova, M. Izakovic, *Monatsh. Chem.* **2004**, *135*, 5–12.
[20] R. Sipos, J. Sima, P. Tarapcik, B. Gyurcsik, *Chem. Pap. - Chem. Zvesti* **2008**, *62*, 496–503.
[21] K. Tsuchiya, K. Akai, A. Tokumura, S. Abe, T. Tamaki, Y. Takiguchi, K. Fukuzawa, *Biochim. Biophys. Acta Gen. Subj.* **2005**, *1725*, 111–119.
[22] S. Kiani, A. Tapper, R. J. Staples, P. Stavropoulos, *J. Am. Chem. Soc.* **2000**, *122*, 7503–7517.
[23] B. V. Nonius, *Kappa CCD Operation Manual*, Delft, The Netherlands, **1997**.
[24] G. M. Sheldrick, *SHELXL97: Program for the Refinement of Crystal Structures*, University of Göttingen, Germany, **1997**.
[25] The Crystalbuilder ProjectR. Welter, *Acta Crystallogr., Sect. A* **2006**, *62*, s252.

Received: April 27, 2009
Published Online: July 24, 2009

